SMAD3 mutation in LDS3 causes bone fragility by impairing the TGF-β pathway and enhancing osteoclastogenesis

Ahmed El-Gazzar [a,1], Heeseog Kang [b,1,2], Nadja Fratzl-Zelman [c,d], Emma Webb [e,f], Aileen M. Barnes [b], Milena Jovanovic [b], Sarju G. Mehta [g], Vipan Datta [e], Vrinda Saraff [h], Ryan K. Dale [i], Frank Rauch [j,k], Joan C. Marini [b], Wolfgang Högler [a,l,*]

[a] Department of Paediatrics and Adolescent Medicine, Johannes Kepler University Linz, Linz, Austria
[b] Section on Heritable Disorders of Bone and Extracellular Matrix, Eunice Kennedy Shriver National Institute of Child Health and Human Development, National Institutes of Health, Bethesda, MD, USA
[c] Ludwig Boltzmann Institute of Osteology at Hanusch Hospital of OEGK and AUVA Trauma Centre Meidling, 1st Medical Department Hanusch Hospital, Vienna, Austria
[d] Vienna Bone and Growth Center, Vienna, Austria
[e] Department of Paediatrics, Jenny Lind Children's Hospital, Norfolk and Norwich University Hospital NHS Foundation Trust, Norwich, UK
[f] Norwich Medical School, University of East Anglia, Norwich, UK
[g] East Anglian Regional Medical Genetics Service, Addenbrookes Hospital, Cambridge, UK
[h] Department of Endocrinology and Diabetes, Birmingham Women's and Children's Hospital NHS Foundation Trust, Birmingham, UK
[i] Bioinformatics and Scientific Programming Core, Eunice Kennedy Shriver National Institute of Child Health and Human Development, Bethesda, MD, USA
[j] Shriners Hospital for Children-Canada, Montreal, QC H4A 0A9, Canada
[k] Department of Human Genetics, McGill University, Montreal, QC H3A 0C7, Canada
[l] Institute of Metabolism and Systems Research, University of Birmingham, Birmingham, UK

ARTICLE INFO

ABSTRACT

Loss-of-function mutations in SMAD3 cause Loeys-Dietz syndrome type 3 (LDS3), a rare autosomal-dominant connective tissue disorder characterized by vascular pathology and skeletal abnormalities. Dysregulation of TGF-β/SMAD signaling is associated with abnormal skeletal features and bone fragility. To date, histomorphometric and ultrastructural characteristics of bone with SMAD3 mutations have not been reported in humans and the exact mechanism by which SMAD3 mutations cause the LDS3 phenotype is poorly understood. Here, we investigated bone histomorphometry and matrix mineralization in human bone with a SMAD3 mutation and explored the associated cellular defect in the TGF-β/SMAD pathway in vitro. The index patient had recurrent fractures, mild facial dysmorphism, arachnodactyly, pectus excavatum, chest asymmetry and kyphoscoliosis. Bone histomorphometry revealed markedly reduced cortical thickness (−68 %), trabecular thickness (−32 %), bone formation rate (−50 %) and delayed mineralization. Quantitative backscattered electron imaging demonstrated undermineralized bone matrix with increased heterogeneity in mineralization. The patient's SMAD3 mutation (c.200 T > G; p.I67S), when expressed from plasmid vectors in HEK293 cells, showed reduced phosphorylation and transcription factor activity compared to normal control and SMAD3 (p.S264Y), a gain-of-function mutation, somatic mosaicism of which causes melorheostosis. Transfection study of the patients' SMAD3 (p.I67S) mutation displayed lower luciferase reporter activity than normal SMAD3 and reduced expression of TGF-β signaling target genes. Patient fibroblasts also demonstrated impaired SMAD3 protein stability. Osteoclastogenic differentiation significantly increased and osteoclast-associated genes, including ACP5 (encoding TRAP), ATP6V0D2, and DCSTAMP, were up-regulated in CD14 (+) peripheral blood mononuclear cells (PBMCs) with the SMAD3 (p.I67S) mutation. Upregulation of osteoclastogenic genes was associated with decreased expression of TGF-β signaling target genes. We conclude that bone with the SMAD3 (p.I67S) mutation features reduced bone formation, and our functional studies revealed decreased SMAD3 activation and protein stability as well as increased osteoclastogenesis. These findings enhance our understanding of the pathophysiology of LDS3

caused by *SMAD3* mutations. Emerging therapies targeting in the TGF-β/SMAD pathway also raise hope for treatment of LDS3.

1. Introduction

Loeys-Dietz syndrome (LDS, OMIM# 609192, 610168, 613795, 614816, 615582), a rare and heterogeneous autosomal dominant connective tissue disorder, was first described in 2005 (Loeys et al., 2005; Loeys et al., 2006). LDS is characterized by severe vascular pathology such as aneurysms, arterial tortuosity, craniofacial features including, bifid uvula, hypertelorism, cleft palate and connective tissue abnormalities such as pectus carinatum/excavatum, scoliosis, joint laxity, arachnodactyly and clubfeet (Erkula et al., 2010). In addition, LDS patients are at increased risk of early onset osteoarthritis, fractures, and delayed bone healing (Gallo et al., 2014; Horbelt et al., 2010; Kirmani et al., 2010; Shen et al., 2014; Tan et al., 2013). Substantial morbidity and mortality have been reported in individuals affected by LDS, mainly caused by arterial (particularly aortic) dissection and rupture (Loeys et al., 2006). To date, mutations in six genes (*TGFBR1, TGFBR2, SMAD2, SMAD3, TGFB2, and TGFB3)* are known to cause LDS (Loeys et al., 2005; Bertoli-Avella et al., 2015; Boileau et al., 2012; Lindsay et al., 2012; Micha et al., 2015; van de Laar et al., 2011). *SMAD3* mutations are causative in 5–10 % of LDS; this subtype is referred to as LDS type 3 (LDS3; OMIM #610168) (van de Laar et al., 2011; Meester et al., 2017). Compared to LDS1 and 2 (mutations in *TGFBR1* and *TGFBR2*, respectively*),* the phenotype of patients with LDS3 includes fewer skeletal manifestations and later onset of aortic and arterial disease (Chesneau et al., 2020; Hostetler et al., 2019; Schepers et al., 2018).

The *SMAD3* gene (OMIM#603109) consists of nine exons and encodes the SMAD3 protein, which is a regulatory SMAD (R-SMAD) of the canonical TGF-β signaling cascade (Schepers et al., 2018). Upon engaging TGF-β ligands binding to the transmembrane receptor complex TGFβRI/TGFβRII, SMAD3 is phosphorylated at the serine residues within the conserved SSxS motif at the carboxy-terminus and forms an oligomeric complex with co-SMAD, SMAD4, and enters the nucleus, where it regulates the transcription of TGF-β target genes (Brown et al., 2007; Derynck and Zhang, 1996; Feng and Derynck, 2005; Massague et al., 2005; Zhang, 2009). The TGF-β/SMAD signaling cascade is important for embryonic development and postnatal homeostasis of the skeleton, but the underlying mechanism is incompletely understood (Wu et al., 2016). Somatic gain-of-function *SMAD3* mutations cause melorheostosis, a sporadic sclerotic dysostosis with distinct local excessive bone formation. Such activating *SMAD3* mutations increase TGF-β signaling inhibiting osteoblast proliferation and stimulating osteoblast differentiation. Thus, melorheostosis may represent an opposing bone phenotype to inactivating *SMAD3* mutations in LDS3 (Kang et al., 2020). *Smad3* knockout mice are osteopenic, with reduced cortical and trabecular parameters, and increased osteocyte density. Bone formation and mineralization rates are impaired. TGF-β-mediated osteoblast proliferation is intact, but TGF-β is unable to suppress osteoblast differentiation, which in turn leads to increased osteoblast and osteocyte apoptosis (Borton et al., 2001). Another *Smad3* knockout mouse model displayed intervertebral disc degeneration during growth due to reduced canonical TGF-β signaling and decreased proteoglycan and collagen content in intervertebral discs (Li et al., 2009).

To date, the ultrastructural bone phenotype of humans affected by LDS3 is unknown. In addition, the mechanism of bone disease caused by human *SMAD3* mutations is incompletely understood. Here, we report *in vivo* bone tissue characteristics and matrix mineralization from an affected patient and the results of *in vitro* functional assessment of the TGF-β signaling pathway to elucidate bone pathophysiology of LDS3.

2. Materials and methods

2.1. Clinical data

Clinical information and anthropometric data were collected from medical records of the index case who attended specialist clinics at Birmingham Children's Hospital (Birmingham, UK) and the Norfolk and Norwich University Hospital (Norwich, UK). Blood, skin and bone biopsy, and DNA samples were collected from the patient and family members as part of routine care after obtaining informed consent/ assent. Bone densitometry, including lateral vertebral assessment (GE Lunar iDXA) and X-rays, were performed as part of routine clinical care. The transiliac bone biopsy was taken following double-labeling with tetracycline for static and dynamic measurement of bone metabolism (patient was naive to bisphosphonate therapy). Clinical information of further affected family members was obtained as part of medical history and informed consent was obtained for publication.

2.2. Bone histomorphometry

Sample preparation and histomorphometric analyses of undecalcified specimen were performed at the Shriner's Hospital for Children, Montreal, Canada, as described (Glorieux et al., 2000). Results were compared to the average values of the age- and sex-specific reference range as established in the same laboratory (Glorieux et al., 2000).

2.3. Bone Mineralization density distribution

Bone Mineralization Density Distribution (BMDD) was assessed by quantitative backscattered electron imaging (qBEI) at the Ludwig Boltzmann Institute of Osteology, Vienna, Austria. as reported previously (Roschger et al., 1998; Roschger et al., 2008). The residual sample block prepared for bone histomorphometry was ground and polished in order to obtain a plane parallel surface and the sample was coated with a thin carbon layer. qBEI was performed on a digital scanning electron microscope equipped with a four-quadrant semiconductor BE detector (DSM 962, Zeiss, Oberkochen Germany). The entire cross-sectioned bone sample area was scanned with a spatial resolution of 3.6 μm/ pixel, gray-level histograms were obtained and converted into weight percent calcium (wt% Ca) histograms. The following BMDD parameters are reported separately for the trabecular and cortical compartment (arithmetic mean of both cortices): the average calcium content (CaMean, wt% Ca); the most frequently occurring calcium concentration (CaPeak, wt% Ca); the heterogeneity in mineralization (CaWidth, Δ wt% Ca) obtained as the full width at half maximum of the BMDD peak; the fraction of lowly (<17.68 wt% Ca) mineralized bone tissue (CaLow); and the fraction of highly-mineralized (>25.30 wt% Ca) bone tissue (CaHigh) and compared with reference values from healthy children (Fratzl-Zelman et al., 2009).

2.4. Cell culture and transfection

HEK293 cells (American Type Culture Collection) were maintained in DMEM base media supplemented with 10 % FBS (Gemini Bio-Products, NC), 100 μg/ml streptomycin, and 100 U/ml penicillin (Gibco). Cells were cultured at 37 °C and 5 % CO_2 and were sub-cultured upon reaching 80 % confluence. For transfection, 2.5×10^5 cells were seeded in 12-well plates in triplicates per each condition. The following day, cells were transfected for 24 h with X-tremeGENE™ HP DNA Transfection Reagent (6,366,236,001, Sigma-Aldrich) and 1 μg/well plasmid DNA constructs expressing pcDNA3.1/NT-GFP-TOPO™
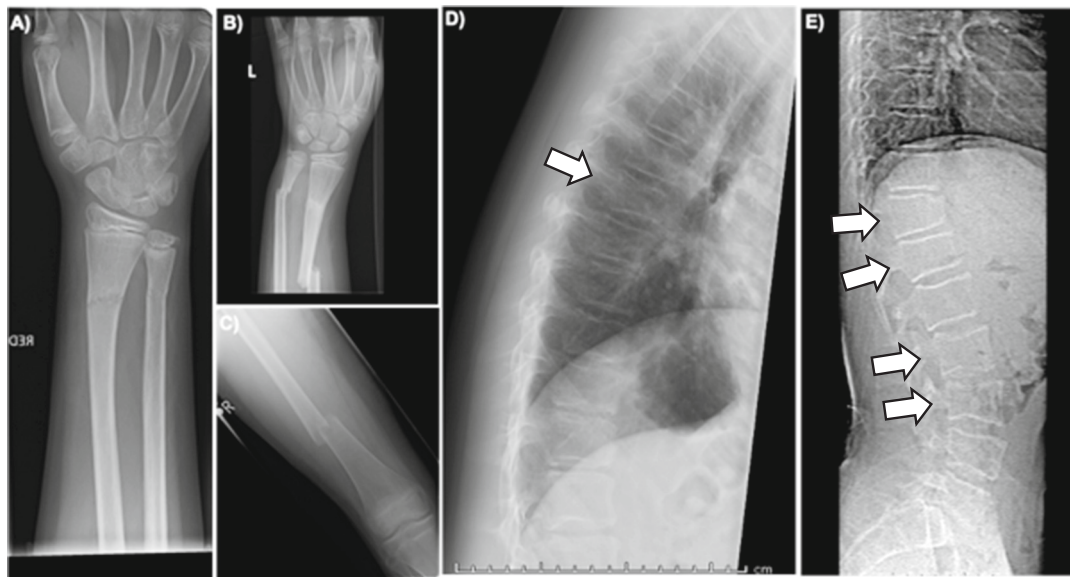
Fig. 1. Radiographs of index case.
Increased bone fragility is demonstrated by recurrent left forearm fractures (at age 13 [A] and 14 [B]), the left femur fracture (age 15 [C]) and vertebral height reductions in the thoracic spine (age 15 [D]) and lumbar spine (age 19 [E]) marked by white arrows.

(K481001, NT-GFP Fusion TOPO™ Expression Kit, Invitrogen™), CS2 Flag-SMAD3 (14052, Addgene), and mutant CS2 Flag-SMAD3 (p.I67S). After transfection, cells were stimulated with 5 ng/mL of TGFβ-1 (7754-BH, R&D) for another 24 h and harvested for RNA.

2.5. Western blot

Cultured and treated cells were lysed in RIPA buffer supplemented with protease and phosphatase inhibitors (ThermoFisher Scientific, Waltham, MA). Proteins in cell lysates were separated on 4–15 % polyacrylamide gels and subjected to western blot analysis. The following primary and secondary antibodies were used for western blotting: phospho-Smad3 (Ser423/425) rabbit polyclonal antibody (#600–401-919; Rockland Inc.), SMAD3 (C67H9) rabbit monoclonal antibody (#9523; Cell Signaling Technology), SMAD2/3 (D7G7) XP® rabbit monoclonal antibody (#8685; Cell Signaling Technology), β-Actin (AC-15) mouse monoclonal antibody (#A5441; Sigma), and FLAG (M2) mouse monoclonal antibody (#F1804; Sigma). Secondary antibodies (LI-COR Biosciences) were IRDye 680RD anti-rabbit IgG (#926-68071) or IRDye 800CW anti-mouse IgG (#926-32210). Blots were visualized on a LI-COR Odyssey infrared imager (LI-COR, Lincoln, NE).

2.6. Plasmid vectors and Luciferase assay

HEK293 cells were co-transfected with following the plasmids: SMAD3-expressing plasmids (normal or p.I67S), pARE-Lux, and pRL Renilla-Luc (Promega, Madison, WI). pARE-Lux vector has 3 copies of ARE (activin-response element), to which SMAD3 binds to induce downstream gene expression (firefly Luciferase, in this vector). Renilla luciferase is used as an internal control to normalize firefly luciferase in plasmid transfection. SMAD3 (p.I67S) mutant plasmid was generated by site-directed mutagenesis using an In-Fusion kit (Takara Bio), with plasmid CS2-Flag-SMAD3 (normal) as a template for PCR. The primer pairs to introduce each mutation were as follows. SMAD3 (p.I67S) forward: 5′-ACCAAGTGCATCACCAGCCCCAGGTCCCTGGATGGCCGGTT-3′, SMAD3 (p.I67S) reverse: 5′-TCCAGGGACCTGGGGCTGGTGATGCACTTGGTGTTGACGTT-3′. The plasmid constructs were verified by Sanger sequencing. CS2 Flag-Smad3 (Addgene plasmid # 14052; http://n2t.net/addgene:14052; RRID: Addgene_14052) and pARE-Lux

(Addgene plasmid # 11768; http://n2t.net/addgene:11768; RRID: Addgene_11768) were a gift from Joan Massague and Jeff Wrana (Cancer Biology and Genetics Program, Memorial Sloan-Kettering Cancer Center, New York, NY) (Kretzschmar et al., 1999; Wrana et al., 1992). Cells were co-transfected with plasmid vectors: pCMV-Flag-SMAD3 for SMAD3, pARE-Lux, and Renilla-Luc. Twenty-four hours after transfection, cells were treated with recombinant human TGF-β1 for 24 h. Cell lysates were subjected to luciferase assay following the manufacturer's instruction (Promega, Madison, WI).

2.7. RNA extraction and real-time quantitative PCR (RT-qPCR)

Total RNA was extracted using the RNeasy Mini kit (Qiagen, Hilden Germany) following the manufacturer's instruction. Genomic DNA was removed from RNA extracts by on-column DNase digestion. Synthesis of cDNA was performed using 500 ng of total RNA and iScript reverse transcription Supermix in 10 μl reverse transcription (RT) reaction (Bio-Rad, Hercules, CA), following the manufacturer's instructions. Comparative real-time qPCR was performed using TaqMan Universal PCR Master Mix in triplicate in Applied Biosystems Prism 7500 Fast Sequence Detection System, according to the manufacturer's instructions. TaqMan probes and primers were purchased from Applied Biosystems: Human *COL1A1* (Hs00164004_m1), *SERPINE1* (Hs00167155_m1), *CCN2* (CTGF) (Hs00170014_m1), *MMP2* (Hs01548727_m1), *ACP5* (Hs00356261_m1), *ATP6V0D2* (Hs01084784_m1), *DCSTAMP* (Hs00229255_m1), and *TGFB1* (Hs00998133_m1). Human *GAPDH* (Hs02786624_g1) and *TBP* (Hs00427620_m1) were used as endogenous controls for normalization of real-time qPCR in osteoclast RNA and human *GAPDH* (Hs02758991_g1) was used as an endogenous control for normalization of gene expression in SMAD3-transfected cells. Relative expression was calculated using the comparative ΔΔCt method.

2.8. SMAD3 stability assay

Human dermal fibroblasts were grown to near confluence in DMEM containing 10 % FBS and 1 % Penicillin/Streptomycin (P/S). The culture medium was replaced with DMEM containing 10 % FBS, 1 % P/S and 50 μg/ml cycloheximide (Sigma-Aldrich, St. Louis, MO) for the number of hours specified. Cycloheximide treatment in DMEM with 10 % FBS, was

Table 1

Bone tissue characteristics of the index case, proband IV.2 (age at biopsy: 15.6 years).

Bone histomorphometry			
Parameters	Reference values (14–16.9 years) (27)	proband IV.2	Difference *versus* controls
Cortical Width (Ct.Wi) μm	1178 (349)	384	−67.5 %
Trabecular thickness (Tb. Th) μm	157 (22)	107	−31.8 %
Osteoid Thickness (O·Th) μm	6.3 (1.0)	5.8	−7.9 %
Osteoblast Surface/Bone Surface (Ob.S/BS) %	7.9 (4.1)	5.3	−32.9 %
Mineralizing Surface/Bone Surface (MS/BS) %	12.5 (3.4)	7.1	−43.2 %
Mineralization lag time (Mlt) d	15.3 (3.6)	25.3	+65.3 %
Bone formation rate/bone surface (BFR/BS) μm³/ μm²/y	37 (10)	18.4	−50.3 %
Eroded surface/bone surface (ES/BS) %	18 (6)	10	−44.4 %

qBEI trabecular bone			
Parameters	Reference values (1.5–23 years) (30)	proband IV.2	Difference *versus* controls
CaMean [wt% Ca]	20.95 (0.57)	18.78	−10.4 %
CaPeak [wt% Ca]	21.66 (0.52)	19.41	−10.4 %
CaWidth [Δwt% Ca]	3.47 [3.12; 3.64]	4.33	+24.8 %
CaLow [% bone area]	6.14 [4.90; 7.99]	23.11	+275 %
CaHigh [% bone area]	0.89 [0.43; 1.47]	0.26	−70.8 %

qBEI cortical bone			
Parameters	Reference values (1.5–23 years) (30)	proband IV.2	Difference *versus* controls
CaMean [wt% Ca]	20.31 (0.93 %)	17.89	−11.9 %
CaPeak [wt%Ca]	21.14 [20.62; 21.75]	18.75	−11.3 %
CaWidth [Δwt% Ca]	3.81 [3.38; 4.38]	4.54	+19.2 %
CaLow [% bone area]	9.06 [6.22; 15.00]	37.02	+300.8 %
CaHigh [% bone area]	0.46 [0.28; 1.22]	0.14	−69.6 %

Data are presented as mean ($\pm$ SD) or median with interquartile range [25th; 75th].

refreshed at 24 h for the longer time points. At harvest, cells were washed with PBS and lysed in RIPA buffer containing protease and phosphatase inhibitors.

2.9. Human CD14 (+) PBMC isolation and osteoclast culture

CD14(+) peripheral blood mononuclear cells (PBMCs) were isolated from blood samples from the index case (proband IV.2) and a healthy donor by density gradient separation using Histopaque-1077 (Sigma-Aldrich). After MACS (magnetic-activated cell sorting) using anti-human CD14 microbeads (Miltenyi Biotech Inc. Auburn, CA), CD14 (+) PBMCs were cultured at a concentration of 3×10^6 cells/ml in low glucose DMEM supplemented with 10 % FBS (Gemini Bio-Products, NC), recombinant human M-CSF (20 ng/ml, R&D Systems, Minneapolis, MN), and recombinant human RANKL (10 ng/ml, R&D Systems). The medium was refreshed every 2 days for total of 6 days. At the end of the culture, the cells were fixed and subjected to tartrate-resistant acid phosphatase (TRAP) staining using a leukocyte acid phosphatase kit (Sigma-Aldrich).

2.10. Statistical analysis

Analysis of RT-qPCR data used the delta-delta Ct method (Livak and Schmittgen, 2001) as implemented in the R "pcr" package (Ahmed and Kim, 2018) followed by Benjamini-Hochberg multiple testing correction of the p-values. Ct values of two technical replicates were averaged for each of the 3 biological replicates within an experiment. For each gene, a comparison between control and stimulated conditions was performed with the pcr::pcr_test function using *GAPDH* as the reference gene, control as the reference condition, and using the default testing method of a *t*-test. The resulting p-values from *t*-tests for each gene were adjusted using the Benjamini-Hochberg multiple testing correction as implemented in the R "p.adjust" function.

For Figs. 3B and 4B, the assays involved biological replicates ($n = 3$) and differences between groups were evaluated with the Student's t-test using a two-tailed distribution. Fig. 5 was not subjected to statistical analysis since $n = 1$ with technical triplicates.

3. Results

3.1. Subject characteristics

3.1.1. Extended family history

The pedigree of this three-generation family is depicted on Supplementary Fig. 1. The father (III.2) of the index case (IV.2) first presented in childhood (age 15 years) with progressive scoliosis. On examination at age 43 years he had low set ears, high arched palate with normal uvula, pectus excavatum, chest asymmetry and kyphoscoliosis, myopia and arachnodactyly without joint hypermobility. Final adult height was 186 cm (91st centile) and weight was 88.9 kg (89th centile).

Cardiology assessment at 15 years, performed due to his Marfanoid phenotype, was unremarkable. At age 42, he presented acutely with a type A aortic dissection and underwent emergency aortic root and valve replacement with left coronary artery re-implantation. He subsequently had dissection of his right coronary artery at age 43 years. He continues to have regular vascular surveillance and has a stable aneurysmal dilatation of his left carotid. At age 47 and 48, he had two separate episodes of streptococcal septicaemia.

From a bone fragility perspective, he had a fractured neck of his left humerus at age 8 years, and had a high impact left tibial fracture at age 15 whilst playing football. He was noted to have a lumbar scoliosis primary curve to the right with marked rotational deformity between T12 and L3. At age 42 years, dual-energy X-ray absorptiometry (DXA) parameters were in the normal range (bone mineral density left hip Z score -1.1, femoral neck Z score -0.3) with normal vertebral height on lateral spine radiograph.

At age 51, Next-Generation Sequencing identified a c.200T>G, p. I67S *SMAD3* variant of uncertain significance which *in silico* prediction classified as likely disease-causing. Since segregation analysis identified further four affected individuals across three generations in the family (Supplementary Fig. 1) and the c.200T>G *SMAD3* variant had previously been reported in two unrelated individuals with LDS3 (Arno et al., 2012), this variant was classified as likely pathogenic.

The paternal grandfather (II.2) was diagnosed with dilatation of aortic root and ascending aorta at age 71 as well as mild to moderate aortic regurgitation and mitral valve prolapse with mild regurgitation, which remained stable until his death at age 79 from aspiration pneumonia and dementia. He was also noted to have scoliosis and arachnodactyly and shared the familial *SMAD3* variant.

Following their father's (III.2) aortic dissection, his children (IV.1 and IV.2 [index case]) were referred for assessment and confirmed to inherit the familial *SMAD3* variant. IV.1 has selective mutism and
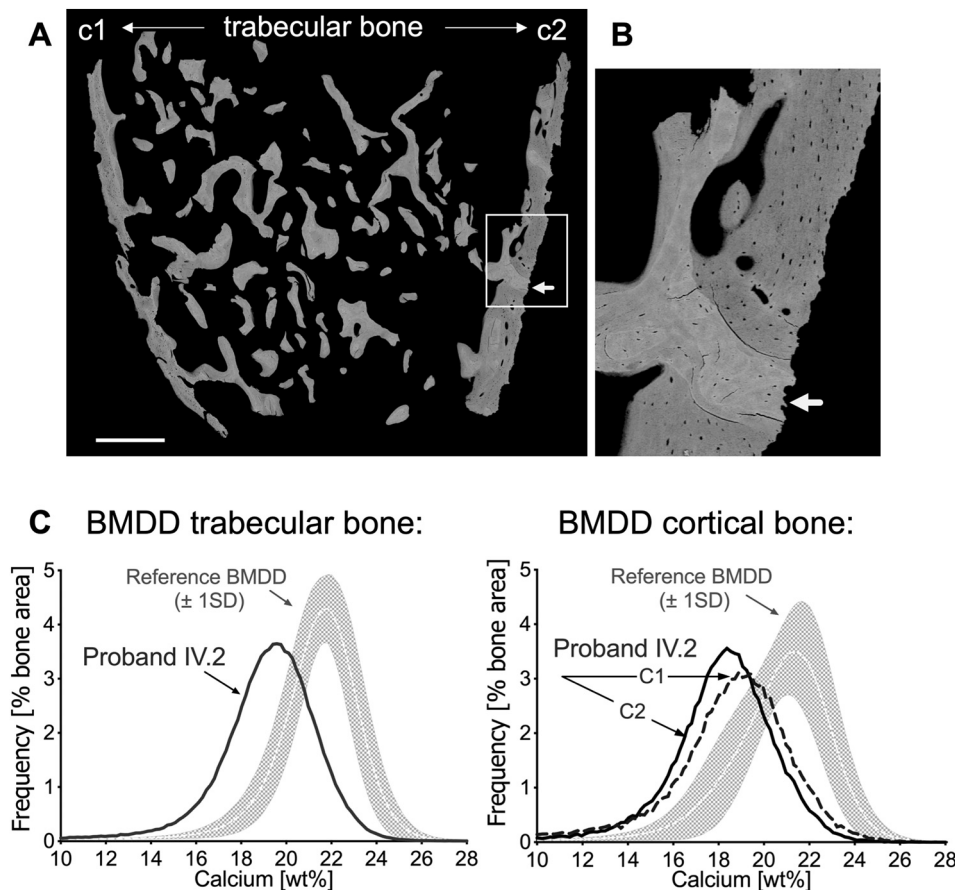
Fig. 2. qBEI results from the transiliac bone biopsy sample from proband IV.2.

(A) Backscattered electron microscopy overview image of the entire sectional area of the bone biopsy sample consisting of two cortices (C1 and C2) and trabecular bone area. (B) Detail of C2 within the white rectangle, showing typical features of lateral modeling drift of the inner cortex during skeletal growth: remnants of higher mineralized trabecular features (bright, white arrow) which became incorporated into newly formed, thus, lower mineralized (grayish) bone matrix. Note, along all the periosteal surface the shallow scalloped erosion mirroring intense bone resorption on the outer cortex (Parfitt et al., 2000). (C) Bone mineralization density distribution (BMDD) of the patient in comparison to reference BMDD of trabecular and cortical bone from healthy children (gray band). Compared to the reference BMDDs, the curves of the patient are shifted to the left, towards lower mineral content of the bone matrix. Note that C2 (solid line), identified as inner cortex is lower mineralized than C1 (broken line), consistent with the presence of a substantial amount of young, thus lowly mineralized, bone tissue in between unresorbed trabecular features (Fratzl-Zelman et al., 2009).

autistic spectrum disorder and does not leave his home. At age 9, he had mild pectus excavatum, scoliosis, high arched palate, easy bruising and hypermobility but no evidence of aortic dilatation. At age 10 years he had a fracture of his left distal radius after an unwitnessed fall. His height was 144 cm (95th centile) and weight 38.2 kg (90th centile). Due to his severe anxiety, he could not be examined again.

3.2. Index case

This individual (IV.2) was most recently seen at 20 years of age. IV.2 was 7 years of age at the time of initial assessment. He was born large for gestational age (birth weight 4.6 kg) at term by normal delivery and had an uneventful neonatal period. He achieved normal developmental milestones. He has normal dentition, hearing and ophthalmology examination and no orofacial features of Marfan syndrome, LDS or vascular Ehlers-Danlos syndrome apart from a short uvula. He has pes planus, moderate pectus excavatum, high arched palate, dolicocephaly, dolichostenomelia, skin translucency and joint hypermobility. He has tall stature (final height 194 cm, 99th centile) and BMI SDS -0.65 and a normal spine with no clinical evidence of scoliosis. He developed an anxiety disorder at age 12 and was diagnosed with autism at age 14, with selective mutism. Echocardiography identified mild aortic root dilatation from age 7 years which remains under close review. He had a trial of Atenolol and Losartan which was discontinued due to poor tolerability. At age 20, maximum aortic root diameter is 43 mm with good biventricular function and no significant valvular abnormalities.

From a bone perspective, his joint hypermobility led to left shoulder subluxation at age 3, which remains an ongoing problem. His first fracture at age 13 was of a left distal ulna and radius fracture with appropriate force, which refractured age 14. At age 15, he had a right spontaneous femoral mid-shaft fracture, whilst standing. At the same

time, he developed intermittent lower backache and lateral vertebral radiograph showed superior end plate fracture of T4 and T6; there was no evidence of cervical spine instability on flexion/extension views. At age 15.6, he had a diagnostic transiliac bone and skin biopsy and DXA showed low lumbar spine bone mineral apparent density (BMAD; Z-score -2.3). Age 19, lateral vertebral assessment showed additional vertebral height reductions at L2-4 (Fig. 1). At age 20, he had two metatarsal stress fractures secondary to walking 60 mins daily. He received three doses of zoledronic acid between 16 and 18 years of age. Lumbar spine BMAD Z-score increased from -2.3 at age 15.7 to 0.1 at age 21. Testosterone was in the normal range (16.6 nmol/L) aged 19 years.

3.3. Bone tissue characteristics

Histomorphometric analysis of IV.2 demonstrated markedly reduced cortical width (Ct.Wi: -67.5 %), trabecular thickness (Tb.Th: -31.8 %), osteoblast surface/bone surface (Ob.S/BS: -32.9 %), mineralizing surface/bone surface (MS/BS: -43.2 %) and bone formation rate/bone surface (BFR/BS: -50.3 %). Bone volume (BV/TV) could not be assessed due to sample fracture. Mineralization lag time (Mlt) was also increased by 65.3 %, with normal osteoid volume. Eroded surface/bone surface (ES/BS: -44.4 %) was also reduced in trabecular bone. qBEI demonstrated a substantially undermineralized bone matrix in both trabecular and cortical bone compartments (arithmetic mean of both cortices), which is mirrored by the decrease in CaMean (-10.4 %, -11.9 % respectively), CaPeak (-10.4 %, -11.3 %, respectively) and CaHigh (-70.8 %, -69.6 % respectively) and a left-shift in the BMDD curve with an increased proportion of CaLow (+275 %, +300 %, respectively) and increased heterogeneity in mineralization, CaWidth (+24.8 %, +19.25 %, respectively). Moreover, qBEI revealed that one cortex (designated as
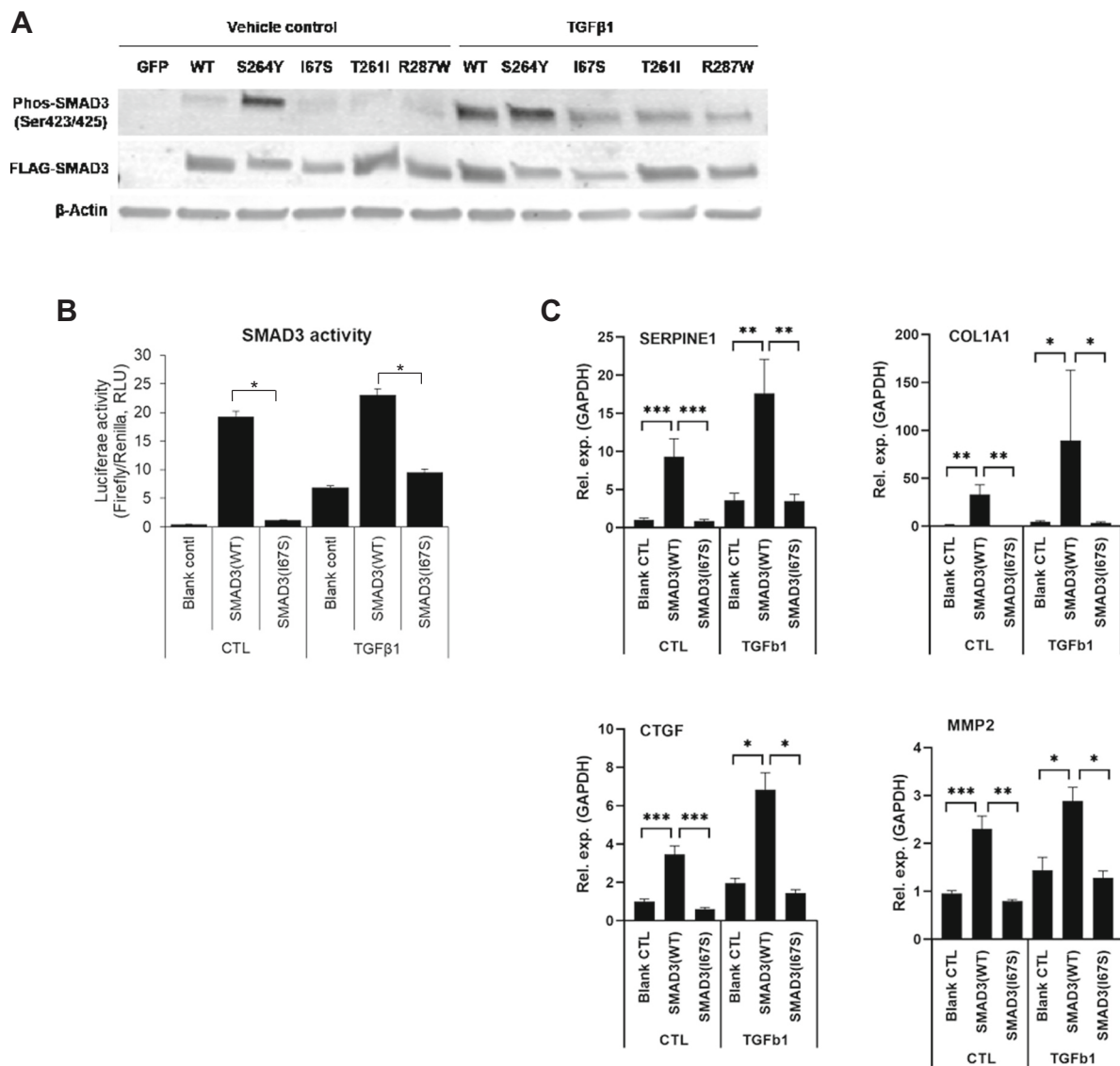
Fig. 3. Plasmid-based expression of SMAD3 (p.I67S) displayed decreased TGF-β signaling and SMAD3 activity.
(A) SMAD3 (p.I67S) was expressed in HEK293 cells and SMAD3 activation was examined after TGF-β1 stimulation. (B) SMAD3 activity assessed by luciferase reporter assay n = 3, * P < 0.05; Student's t-test). Error bars: SD of replicates. (C) Real-time qPCR for expression of TGF-β signaling target genes in HEK293 cells showed reduced TGF-β signaling by the SMAD3 (p.I67S) mutation. n = 3 biological replicates, each with two technical replicates; *, P < 0.05; **P < 0.01, ***P < 0.005.

c1) was more highly mineralized as the other one (c2). C2 is composed of remnants of higher mineralized trabecular features (bright) and new bone matrix that is lower mineralized (dark gray) resulting in an overall lower average matrix mineralization than c1. Moreover, the periosteal surface of c2 showed an irregular surface characterized by shallow scalloped erosions (Table 1 and Fig. 2).

### 3.4. Plasmid-based expression of SMAD3 (p.I67S) displayed decreased TGF-β signaling and SMAD3 activity

The identified *SMAD3* missense mutation c.200T>G is located in exon 1 of the *SMAD3* gene, substituting isoleucine at residue 67 with serine (p.I67S). In order to examine the functionality of the resulting SMAD3 (p.I67S) protein, SMAD3 mutations reported in LDS3 with early-onset osteoarthritis (p.T261I and p.R287W (van de Laar et al., 2011)), a somatic gain-of-function SMAD3 mutation (p.S264Y) causing melorheostosis (Kang et al., 2020), and SMAD3 (p.I67S) were expressed individually in HEK293 cells using plasmid vectors.

We noted that in the absence of TGF-β1 stimulation, the basal level of

SMAD3 phosphorylation was almost undetectable in all transfected cells, except in the gain of function mutant SMAD3 (p.S264Y). Upon stimulation with TGF-β1, the SMAD3 (p.I67S) mutation showed less phosphorylation than normal control (WT) or SMAD3 (p.S264Y) (Fig. 3A). A similar trend was seen with SMAD3 mutations (p.T261I or p. R287W) that previously showed decreased TGF-β/SMAD3 signaling (van de Laar et al., 2011).

To investigate the consequence of the SMAD3 (p.I67S) mutation on TGF-β signal transduction, luciferase reporter assays were performed. We found that cells expressing SMAD3 (p.I67S) displayed significantly lower luciferase activity than normal SMAD3 in the presence or absence of TGF-β1 (Fig. 3B & C).

To further analyze the effect of the SMAD3 (p.I67S) mutation on the TGF-β/SMAD3 signaling, cells were either left untreated or treated with TGF-β1 and target gene expression was determined by real-time quantitative PCR (RT-qPCR). In line with reduced luciferase expression in the luciferase reporter assay, expression of TGF-β/SMAD3 signaling target genes including *SERPINE1*, *COL1A1*, *CCN2* (CTGF), and *MMP2* was reduced in SMAD3 (p.I67S) mutant-expressing cells (Fig. 3B & 3C).
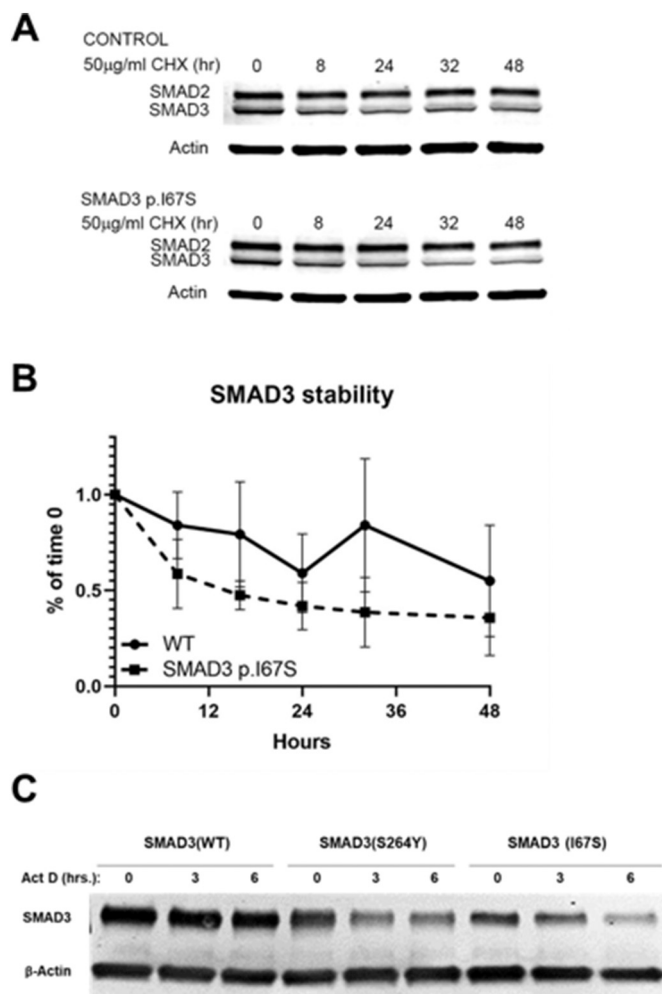
Fig. 4. Reduced SMAD3 protein stability by SMAD3 (p.I67S) mutation. (A) Primary culture of dermal fibroblasts from the index patient with SMAD3 (p.I67S) were treated with cycloheximide and SMAD3 protein stability was examined by western blot analysis. (B) Measurement of SMAD3 protein band intensity. (C) SMAD3 (p.I67S) was expressed in HEK293 cells and SMAD3 protein stability was assessed by western blot analysis after actinomycin D treatment.

3.5. Reduced protein stability induced by SMAD3 (p.I67S) mutation

Next, we investigated the effect of the SMAD3 (p.I67S) mutation on SMAD3 protein stability. Primary dermal fibroblasts were isolated from proband IV.2 and were treated with cycloheximide for different time points ranging from 0 to 48 h. Analysis of SMAD3 (p.I67S) in patient dermal fibroblasts by western blot suggested that SMAD3 stability was decreased (Fig. 4A & B), although the results were not significant. This was shown to be, in fact, the case by transfection of SMAD3 (p.I67S) plasmid vector in HEK293 cells, in which mutant protein displayed less stability than normal SMAD3 (Fig. 4C). These results suggest that the p. I67S mutation decreases available SMAD3 protein and thereby reduces the TGF-β signal transduction.

3.6. SMAD3 (p.I67S) mutation stimulates osteoclastogenesis in vitro

We next investigated the effect of the SMAD3 (p.I67S) mutation on osteoclastogenesis in vitro. CD14(+) PBMCs from patient and an age- and gender matched healthy control were primed with macrophage colony-stimulating factor (M-CSF) and receptor activator of nuclear factor kappa-B ligand (RANKL) to generate osteoclasts in culture. After 6 days,

the number and size of TRAP-positive multinucleated cells (number of nuclei >3) were determined. Cells with the SMAD3 (p.I67S) mutation showed increased formation of TRAP-positive multinucleated osteoclasts in both number and size (Fig. 5A & B). Expression of osteoclast marker genes was determined by performing real-time quantitative PCR analysis of RNA isolated at 0, 4, and 6 days after osteoclastogenic induction by RANKL. Under these culture conditions, multinucleated cells started to appear as early as day 4, and osteoclast formation peaked around day 6. The results showed that osteoclast-associated genes, including *ACP5* (encoding TRAP), *ATP6V0D2*, and *DCSTAMP*, were upregulated in cells isolated from the patient with a SMAD3 (p.I67S) mutation compared with cells from a non-LDS individual (Fig. 5C). Because of the known variability of healthy osteoclast preparations, we cannot conclude that these increases differed significantly from healthy age-matched individuals, although results are suggestive. These results are supported by our finding of reduced TGF-β signaling in the cells with SMAD3 (p.I67S), as displayed by decreased expression of TGF-β signaling target genes in index patient's CD14(+) PBMCs (Fig. 5D).

4. Discussion

The results of this study demonstrate the effect of loss-of-function mutation in *SMAD3* on human bone tissue. Using in vitro mechanistic studies, we confirm decreased TGF-β signaling, which explains the unique bone phenotype of reduced bone formation with thin cortical and trabecular structures and reduced bone matrix mineralization. In addition, our study suggests that decreased SMAD3 function may increase osteoclastogenesis in vitro. Despite that, bone histomorphometry revealed rather low bone turnover in the trabecular compartment, the periosteum surface of the inner cortex showed scalloped erosions, reflecting intense bone resorption. Because during skeletal growth, bone formation and bone resorption are uncoupled and occur on different cortical surfaces, (Le Goff and Cormier-Daire, 2012), it might be that the impaired SMAD3 function leads to a much higher cortical bone removal than bone apposition. Such a dysbalanced bone modeling process will indeed lead to a marked thinning and fragility of the cortices, which is exactly what we observed. In accordance, the positive response to bisphosphonate therapy in this case indicates that anti-resorptive treatment is effective in patients with LDS3.

Smad3-deficient mice display reduced bone mass and bone formation, reduced cortical and trabecular thickness, reduced mineralization and reduced osteoblast differentiation and survival (Borton et al., 2001). These results are in line with our novel human bone biopsy data, with a similar percent reduction in structural histomorphometry. The delayed mineralization (increased Mlt) supports the finding of generally under-mineralized bone matrix demonstrated using qBEI in both cortical and trabecular bone. Our preliminary finding of increased osteoclastogenesis in vitro (approximately 36 % increase in osteoclast number and 72 % increase in area) is also supported by *Smad3* KO mouse data, although results were not significant in that study (Borton et al., 2001). Interestingly, TGF-β2 transgenic mice also show reduced bone mass and increased bone turnover as indicated by increased osteoblast and osteoclast activation (Erlebacher and Derynck, 1996; Erlebacher et al., 1998). On the other hand, mice overexpressing TGF-β dominant negative type II receptor show increased trabecular bone mass due to reduced number of osteoclasts without any change in the rate of bone formation (Filvaroff et al., 1999).

The majority of *SMAD3* mutations in LDS3 are missense variants; splice site variants constitute up to 6 % of cases (Schepers et al., 2018). Despite the absence of mutational hot spot identification in SMAD3, the majority (63 %) lie in the C-terminal MH2 domain, which is responsible for oligomerization with SMAD4 and transcription factor activity (Schepers et al., 2018). Although there is no genotype-phenotype correlation for SMAD3 established (Chesneau et al., 2020), patients with mutations in the MH2 domain may have earlier onset of aortic events than those with mutations in the MH1 region, as in the family presented
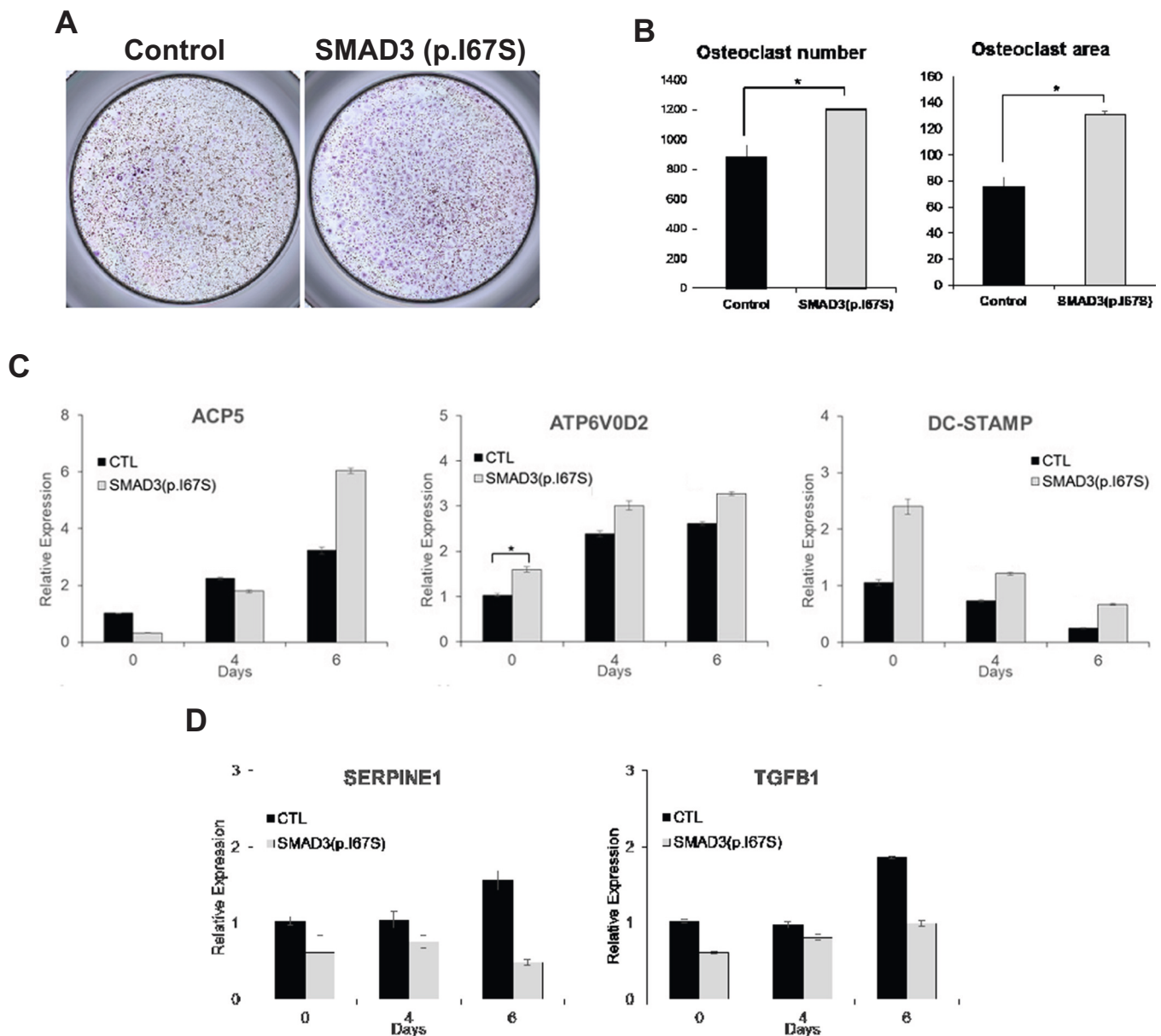
Fig. 5. SMAD3 (p.I67S) mutation stimulated osteoclastogenesis *in vitro*.
(A) CD14(+) PBMCs from patient and age- and gender matched healthy control were cultured in the presence of M-CSF and RANKL. The age of the matched control donor is 22 years old. TRAP staining was performed after 6 days visualized osteoclasts. (B) Measurement of osteoclast number (per well) and area occupied by multinucleated osteoclasts (per well). $n = 3$; *, $P < 0.05$; Student's *t*-test). (C) Increased expression of osteoclast marker genes in osteoclasts by SMAD3 (p.I67S). $n = 1$ with technical replicates, therefore no significance presented (D) Decreased TGF-β signaling in osteoclasts with the SMAD3 (p.I67S) mutation. n = 1 with technical replicates, therefore no significance presented.

here (Schepers et al., 2018).

Patients with LDS present with a vascular phenotype that is considered more severe than in Marfan syndrome. This may occur because the TGF-β signaling pathway has multiple pleotropic functions, compared to a single molecule mutation in the *FBN1* gene as in Marfan syndrome (MacCarrick et al., 2014).

To date, the pathophysiology of TGF-β signaling dysregulation and the mechanism of action in LDS remain poorly understood, since TGF-β signaling (presumably non-canonical) is mostly upregulated despite loss-of-function mutations (Pezzini et al., 2012) in elements of the TGF-β/SMAD signaling cascade, which is referred to as the TGF-β paradox (Massague, 2012). Excess activation of TGF-β signaling in LDS leads to vascular tortuosity and craniofacial and skeletal abnormalities. Excess activation of the TGF-β signaling pathway also stimulates growth plate

chondrogenesis, as seen in Marfan syndrome and other *FBN1* defects (Le Goff and Cormier-Daire, 2012). Affected family members in our family featured tall stature from birth, suggesting that *SMAD3* mutations, *via* increased chondrogenic differentiation, might lead to excessive growth in height.

To investigate the mechanism by which SMAD3 mediates TGF-β signaling in bone remodeling, we expressed the familial SMAD3 mutation (p.I67S) in HEK293 cells. We observed that upon stimulation with TGF-β1, the SMAD3 (p.I67S) mutation associated with LDS3 showed less phosphorylation than normal SMAD3 control. This is in line with the results from the luciferase reporter assay, which showed that SMAD3 (p. I67S) mutant cells expressed lower luciferase reporter activity when compared to cells expressing normal SMAD3.

In conclusion, our results add to the understanding of the molecular

mechanism of the TGF-β/SMAD3 signaling pathway in LDS3 in humans. Although lack of additional matched controls limits the strength of our data, we showed that SMAD3 (p.I67S) results in decreased TGF-β signaling and, potentially, also increased osteoclastogenesis, likely due to reduced SMAD3 activity and protein stability. These defects cause a bone fragility phenotype with reduced bone formation and mineralization. Results are similar to the *Smad3* KO mouse model. Loss of SMAD3 activity likely decreases bone formation and mineralization and increases osteoclastogenesis by modulating the transcriptional activity of TGF-β target genes. Since activating (somatic) and inactivating *SMAD3* mutations are associated with high and low bone mass phenotypes, respectively, drug targets within the TGF-β/SMAD pathway may lend themselves to new targeted therapeutic options. A promising agent in this regard is losartan, an angiotensin II type 2 receptor blocker, known to reduce the expression of TGF-β ligand, receptors, and activators. Losartan therapy improved bone pain and total BMD in a girl with Camurati-Engelmann syndrome (*TGFB1* mutation) (Ayyavoo et al., 2014). Further hope for treatment lies in the TGF-β neutralizing antibody, Fresolimumab, which is in clinical trials in children with osteogenesis imperfecta (El-Gazzar and Hogler, 2021). For now, antiresorptive therapy appears a reasonable first-line of treatment for bone fragility in LDS3.

CRediT authorship contribution statement

AEG, HK, JCM and WH have drafted the manuscript. WH, *VS*, EW, VD and SM provided clinical data, SM arranged genetic analysis, *VS* and WH conducted the bone biopsy. FR performed histomorphometry analysis and NF-Z qBEI analysis. HK, AMB, MJ and JCM conducted and analyzed the *in vitro* study. RKD provided statistical analyses. All authors provided intellectual input and approved submission of the manuscript for publication.

Data availability statement

The data that support the findings of this study are available from the corresponding author upon reasonable request.

Declaration of competing interest

The Authors declare that there is no conflict of interest.

Acknowledgments

Appendix A. Supplementary data

Supplementary data to this article can be found online at https://doi.org/10.1016/j.bonr.2022.101603.

References

Ahmed, M., Kim, D.R., 2018. Pcr: an R package for quality assessment, analysis and testing of qPCR data. PeerJ 6, e4473.

Arno, G., Aragon-Martin, J.A., Song, O., Kamali, N., Saggar-Malik, A.K., Jahangiri, M., Child, A., 2012. Mutations in SMAD3 in a British cohort of thoracic aortic aneurysm and dissection (TAAD) patients. In: Conference: American Society of Human GeneticsAt: San Francisco, California, USA. http://www.ashg.org/2012meeting/abstracts/fulltext/f120120562.htm.

Ayyavoo, A., Derraik, J.G., Cutfield, W.S., Hofman, P.L., 2014. Elimination of pain and improvement of exercise capacity in camurati-engelmann disease with losartan. J. Clin. Endocrinol. Metab. 99, 3978–3982.

Bertoli-Avella, A.M., Gillis, E., Morisaki, H., Verhagen, J.M.A., de Graaf, B.M., van de Beek, G., Gallo, E., Kruithof, B.P.T., Venselaar, H., Myers, L.A., Laga, S., Doyle, A.J., Oswald, G., van Cappellen, G.W.A., Yamanaka, I., van der Helm, R.M., Beverloo, B.,

de Klein, A., Pardo, L., Lammens, M., Evers, C., Devriendt, K., Dumoulein, M., Timmermans, J., Bruggenwirth, H.T., Verheijen, F., Rodrigus, I., Baynam, G., Kempers, M., Saenen, J., Van Craenenbroeck, E.M., Minatoya, K., Matsukawa, R., Tsukube, T., Kubo, N., Hofstra, R., Goumans, M.J., Bekkers, J.A., Roos-Hesselink, J. W., van de Laar, I., Dietz, H.C., Van Laer, L., Morisaki, T., Wessels, M.W., Loeys, B.L., 2015. Mutations in a TGF-beta ligand, TGFB3, cause syndromic aortic aneurysms and dissections. J. Am. Coll. Cardiol. 65, 1324–1336.

Boileau, C., Guo, D.C., Hanna, N., Regalado, E.S., Detaint, D., Gong, L., Varret, M., Prakash, S.K., Li, A.H., d'Indy, H., Braverman, A.C., Grandchamp, B., Kwartler, C.S., Gouya, L., Santos-Cortez, R.L., Abifadel, M., Leal, S.M., Muti, C., Shendure, J., Gross, M.S., Rieder, M.J., Vahanian, A., Nickerson, D.A., Michel, J.B., National Heart, L., Blood Institute Go Exome Sequencing, P., Jondeau, G., Milewicz, D.M., 2012. TGFB2 mutations cause familial thoracic aortic aneurysms and dissections associated with mild systemic features of Marfan syndrome. Nat. Genet. 44, 916–921.

Borton, A.J., Frederick, J.P., Datto, M.B., Wang, X.F., Weinstein, R.S., 2001. The loss of Smad3 results in a lower rate of bone formation and osteopenia through dysregulation of osteoblast differentiation and apoptosis. J. Bone Miner. Res. 16, 1754–1764.

Brown, K.A., Pietenpol, J.A., Moses, H.L., 2007. A tale of two proteins: differential roles and regulation of Smad2 and Smad3 in TGF-beta signaling. J. Cell. Biochem. 101, 9–33.

Chesneau, B., Edouard, T., Dulac, Y., Colineaux, H., Langeois, M., Hanna, N., Boileau, C., Arnaud, P., Chassaing, N., Julia, S., Jondeau, G., Plancke, A., Khau Van Kien, P., Plaisancie, J., 2020. Clinical and genetic data of 22 new patients with SMAD3 pathogenic variants and review of the literature. Mol. Genet. Genomic Med. 8, e1132.

Derynck, R., Zhang, Y., 1996. Intracellular signalling: the mad way to do it. Curr. Biol. 6, 1226–1229.

El-Gazzar, A., Hogler, W., 2021. Mechanisms of bone fragility: from osteogenesis imperfecta to secondary osteoporosis. Int. J. Mol. Sci. 22.

Erkula, G., Sponseller, P.D., Paulsen, L.C., Oswald, G.L., Loeys, B.L., Dietz, H.C., 2010. Musculoskeletal findings of loeys-dietz syndrome. J. Bone Joint Surg. Am. 92, 1876–1883.

Erlebacher, A., Derynck, R., 1996. Increased expression of TGF-beta 2 in osteoblasts results in an osteoporosis-like phenotype. J. Cell Biol. 132, 195–210.

Erlebacher, A., Filvaroff, E.H., Ye, J.Q., Derynck, R., 1998. Osteoblastic responses to TGF-beta during bone remodeling. Mol. Biol. Cell 9, 1903–1918.

Feng, X.H., Derynck, R., 2005. Specificity and versatility in tgf-beta signaling through smads. Annu. Rev. Cell Dev. Biol. 21, 659–693.

Filvaroff, E., Erlebacher, A., Ye, J., Gitelman, S.E., Lotz, J., Heillman, M., Derynck, R., 1999. Inhibition of TGF-beta receptor signaling in osteoblasts leads to decreased bone remodeling and increased trabecular bone mass. Development 126, 4267–4279.

Fratzl-Zelman, N., Roschger, P., Misof, B.M., Pfeffer, S., Glorieux, F.H., Klaushofer, K., Rauch, F., 2009. Normative data on mineralization density distribution in iliac bone biopsies of children, adolescents and young adults. Bone 44, 1043–1048.

Gallo, E.M., Loch, D.C., Habashi, J.P., Calderon, J.F., Chen, Y., Bedja, D., van Erp, C., Gerber, E.E., Parker, S.J., Sauls, K., Judge, D.P., Cooke, S.K., Lindsay, M.E., Rouf, R., Myers, L., Ap Rhys, C.M., Kent, K.C., Norris, R.A., Huso, D.L., Dietz, H.C., 2014. Angiotensin II-dependent TGF-beta signaling contributes to Loeys-Dietz syndrome vascular pathogenesis. J. Clin. Invest. 124, 448–460.

Glorieux, F.H., Travers, R., Taylor, A., Bowen, J.R., Rauch, F., Norman, M., Parfitt, A.M., 2000. Normative data for iliac bone histomorphometry in growing children. Bone 26, 103–109.

Horbelt, D., Guo, G., Robinson, P.N., Knaus, P., 2010. Quantitative analysis of TGFBR2 mutations in marfan-syndrome-related disorders suggests a correlation between phenotypic severity and Smad signaling activity. J. Cell Sci. 123, 4340–4350.

Hostetler, E.M., Regalado, E.S., Guo, D.C., Hanna, N., Arnaud, P., Muino-Mosquera, L., Callewaert, B.L., Lee, K., Leal, S.M., Wallace, S.E., Rideout, A.L., Dyack, S., Aatre, R. D., Boileau, C., De Backer, J., Jondeau, G., Milewicz, D.M., 2019. SMAD3 pathogenic variants: risk for thoracic aortic disease and associated complications from the montalcino aortic consortium. J. Med. Genet. 56, 252–260.

Kang, H., Jha, S., Ivovic, A., Fratzl-Zelman, N., Deng, Z., Mitra, A., Cabral, W.A., Hanson, E.P., Lange, E., Cowen, E.W., Katz, J., Roschger, P., Klaushofer, K., Dale, R. K., Siegel, R.M., Bhattacharyya, T., Marini, J.C., 2020. Somatic SMAD3-activating mutations cause melorheostosis by up-regulating the TGF-beta/SMAD pathway. J. Exp. Med. 217.

Kirmani, S., Tebben, P.J., Lteif, A.N., Gordon, D., Clarke, B.L., Hefferan, T.E., Yaszemski, M.J., McGrann, P.S., Lindor, N.M., Ellison, J.W., 2010. Germline TGF-beta receptor mutations and skeletal fragility: a report on two patients with loeys-dietz syndrome. Am. J. Med. Genet. A 152A, 1016–1019.

Kretzschmar, M., Doody, J., Timokhina, I., Massague, J., 1999. A mechanism of repression of TGFbeta/ smad signaling by oncogenic ras. Genes Dev. 13, 804–816.

van de Laar, I.M., Oldenburg, R.A., Pals, G., Roos-Hesselink, J.W., de Graaf, B.M., Verhagen, J.M., Hoedemaekers, Y.M., Willemsen, R., Severijnen, L.A., Venselaar, H., Vriend, G., Pattynama, P.M., Collee, M., Majoor-Krakauer, D., Poldermans, D., Frohn-Mulder, I.M., Micha, D., Timmermans, J., Hilhorst-Hofstee, Y., Bierma-Zeinstra, S.M., Willems, P.J., Kros, J.M., Oei, E.H., Oostra, B.A., Wessels, M.W., Bertoli-Avella, A.M., 2011. Mutations in SMAD3 cause a syndromic form of aortic aneurysms and dissections with early-onset osteoarthritis. Nat. Genet. 43, 121–126.

Le Goff, C., Cormier-Daire, V., 2012. From tall to short: the role of TGFbeta signaling in growth and its disorders. Am J Med Genet C Semin Med Genet 160C, 145–153.

Li, C.G., Liang, Q.Q., Zhou, Q., Menga, E., Cui, X.J., Shu, B., Zhou, C.J., Shi, Q., Wang, Y. J., 2009. A continuous observation of the degenerative process in the intervertebral disc of Smad3 gene knock-out mice. Spine (Phila Pa 1976) 34, 1363–1369.

Lindsay, M.E., Schepers, D., Bolar, N.A., Doyle, J.J., Gallo, E., Fert-Bober, J., Kempers, M. J., Fishman, E.K., Chen, Y., Myers, L., Bjeda, D., Oswald, G., Elias, A.F., Levy, H.P., Anderlid, B.M., Yang, M.H., Bongers, E.M., Timmermans, J., Braverman, A.C., Canham, N., Mortier, G.R., Brunner, H.G., Byers, P.H., Van Eyk, J., Van Laer, L., Dietz, H.C., Loeys, B.L., 2012. Loss-of-function mutations in TGFB2 cause a syndromic presentation of thoracic aortic aneurysm. Nat. Genet. 44, 922–927.

Livak, K.J., Schmittgen, T.D., 2001. Analysis of relative gene expression data using real-time quantitative PCR and the 2(-Delta Delta C(T)) method. Methods 25, 402–408.

Loeys, B.L., Chen, J., Neptune, E.R., Judge, D.P., Podowski, M., Holm, T., Meyers, J., Leitch, C.C., Katsanis, N., Sharifi, N., Xu, F.L., Myers, L.A., Spevak, P.J., Cameron, D. E., De Backer, J., Hellemans, J., Chen, Y., Davis, E.C., Webb, C.L., Kress, W., Coucke, P., Rifkin, D.B., De Paepe, A.M., Dietz, H.C., 2005. A syndrome of altered cardiovascular, craniofacial, neurocognitive and skeletal development caused by mutations in TGFBR1 or TGFBR2. Nat. Genet. 37, 275–281.

Loeys, B.L., Schwarze, U., Holm, T., Callewaert, B.L., Thomas, G.H., Pannu, H., De Backer, J.F., Oswald, G.L., Symoens, S., Manouvrier, S., Roberts, A.E., Faravelli, F., Greco, M.A., Pyeritz, R.E., Milewicz, D.M., Coucke, P.J., Cameron, D.E., Braverman, A.C., Byers, P.H., De Paepe, A.M., Dietz, H.C., 2006. Aneurysm syndromes caused by mutations in the TGF-beta receptor. N. Engl. J. Med. 355, 788–798.

MacCarrick, G., Black III, J.H., Bowdin, S., El-Hamamsy, I., Frischmeyer-Guerrerio, P.A., Guerrerio, A.L., Sponseller, P.D., Loeys, B., Dietz III, H.C., 2014. Loeys-dietz syndrome: a primer for diagnosis and management. Genet. Med. 16, 576–587.

Massague, J., 2012. TGFbeta signalling in context. Nat Rev Mol Cell Biol 13, 616–630.

Massague, J., Seoane, J., Wotton, D., 2005. Smad transcription factors. Genes Dev. 19, 2783–2810.

Meester, J.A.N., Verstraeten, A., Schepers, D., Alaerts, M., Van Laer, L., Loeys, B.L., 2017. Differences in manifestations of marfan syndrome, ehlers-danlos syndrome, and loeys-dietz syndrome. Ann. Cardiothorac. Surg. 6, 582–594.

Micha, D., Guo, D.C., Hilhorst-Hofstee, Y., van Kooten, F., Atmaja, D., Overwater, E., Cayami, F.K., Regalado, E.S., van Uffelen, R., Venselaar, H., Faradz, S.M., Vriend, G., Weiss, M.M., Sistermans, E.A., Maugeri, A., Milewicz, D.M., Pals, G., van Dijk, F.S.,

2015. SMAD2 mutations are associated with arterial aneurysms and dissections. Hum. Mutat. 36, 1145–1149.

Parfitt, A.M., Travers, R., Rauch, F., Glorieux, F.H., 2000. Structural and cellular changes during bone growth in healthy children. Bone 27, 487–494.

Pezzini, A., Del Zotto, E., Giossi, A., Volonghi, I., Costa, P., Padovani, A., 2012. Transforming growth factor beta signaling perturbation in the loeys-dietz syndrome. Curr. Med. Chem. 19, 454–460.

Roschger, P., Fratzl, P., Eschberger, J., Klaushofer, K., 1998. Validation of quantitative backscattered electron imaging for the measurement of mineral density distribution in human bone biopsies. Bone 23, 319–326.

Roschger, P., Paschalis, E.P., Fratzl, P., Klaushofer, K., 2008. Bone mineralization density distribution in health and disease. Bone 42, 456–466.

Schepers, D., Tortora, G., Morisaki, H., MacCarrick, G., Lindsay, M., Liang, D., Mehta, S. G., Hague, J., Verhagen, J., van de Laar, I., Wessels, M., Detisch, Y., van Haelst, M., Baas, A., Lichtenbelt, K., Braun, K., van der Linde, D., Roos-Hesselink, J., McGillivray, G., Meester, J., Maystadt, I., Coucke, P., El-Khoury, E., Parkash, S., Diness, B., Risom, L., Scurr, I., Hilhorst-Hofstee, Y., Morisaki, T., Richer, J., Desir, J., Kempers, M., Rideout, A.L., Horne, G., Bennett, C., Rahikkala, E., Vandeweyer, G., Alaerts, M., Verstraeten, A., Dietz, H., Van Laer, L., Loeys, B., 2018. A mutation update on the LDS-associated genes TGFB2/3 and SMAD2/3. Hum. Mutat. 39, 621–634.

Shen, J., Li, S., Chen, D., 2014. TGF-beta signaling and the development of osteoarthritis. Bone Res. 2.

Tan, E.W., Offoha, R.U., Oswald, G.L., Skolasky, R.L., Dewan, A.K., Zhen, G., Shapiro, J. R., Dietz, H.C., Cao, X., Sponseller, P.D., 2013. Increased fracture risk and low bone mineral density in patients with loeys-dietz syndrome. Am. J. Med. Genet. A 161A, 1910–1914.

Wrana, J.L., Attisano, L., Carcamo, J., Zentella, A., Doody, J., Laiho, M., Wang, X.F., Massague, J., 1992. TGF beta signals through a heteromeric protein kinase receptor complex. Cell 71, 1003–1014.

Wu, M., Chen, G., Li, Y.P., 2016. TGF-beta and BMP signaling in osteoblast, skeletal development, and bone formation, homeostasis and disease. Bone Res. 4, 16009.

Zhang, Y.E., 2009. Non-Smad pathways in TGF-beta signaling. Cell Res. 19, 128–139.